

Effect of Rotor Geometry and Blade Kinematics on Cycloidal Rotor Hover Performance

Moble Benedict,* Tejaswi Jarugumilli,† and Inderjit Chopra‡

University of Maryland, College Park, Maryland 20742

DOI: 10.2514/1.C031461

This paper describes the systematic performance measurements conducted to understand the role of rotor geometry and blade pitching kinematics on the performance of a microscale cycloidal rotor. Key geometric parameters that were investigated include rotor radius, blade span, chord, and blade planform. Because of the flow curvature effects, the cycloidal-rotor performance was a strong function of the chord/radius ratio. The optimum chord/radius ratios were extremely high, around 0.5–0.8, depending on the blade pitching amplitude. Cycloidal rotors with shorter blade spans had higher power loading (thrust/power), especially at lower pitching amplitudes. Increasing the solidity of the rotor by increasing the blade chord, while keeping the number of blades constant, produced large improvements in power loading. Blade planform shape did not have a significant impact, even though trapezoidal blades with a moderate taper ratio were slightly better than rectangular blades. On the blade kinematics side, higher blade pitching amplitudes were found to improve the power loading of the cycloidal rotor. Asymmetric pitching with a higher pitch angle at the top than at the bottom produced better power loading. The chordwise optimum pitching axis location was observed to be around 25–35% of the blade chord. The power loading of the optimized cycloidal rotor was higher than that of a conventional microrotor.

Nomenclature

A	= cycloidal-rotor rectangular projected area; $2bR$, m ²
b	= blade span, m
c	= blade chord, m
DL	= disk loading; T_{Res}/A , N · m ⁻²
N_b	= number of blades
P	= total aerodynamic power, W
PL	= power loading; T_{Res}/P , N · W ⁻¹
R	= radius of rotor, m
Re	= Reynolds number
R'	= distance of arbitrary point on blade chord from rotor axis, m
T_{Res}	= resultant thrust, N
T_y	= rotor sideward thrust, N
T_z	= rotor vertical thrust, N
TR	= taper ratio, mid-chord/root-chord for trapezoidal blade planform
X, Y, Z	= rotor coordinate system, m
x	= distance of arbitrary point on blade chord behind blade pitching axis, m
α_x	= angle between velocity vector and blade chord at arbitrary chordwise location, deg
α_1	= angle between velocity vector and blade chord at blade leading edge, deg
α_2	= angle between velocity vector and blade chord at blade trailing edge, deg
θ	= blade pitch angle, deg
ρ	= air density, kg · m ⁻³
σ	= rotor solidity; $N_b c / 2\pi R$
ϕ	= phase angle of resultant thrust vector, deg

$$\begin{aligned} \Psi &= \text{azimuthal position of blade, deg} \\ \Omega &= \text{rotational speed of rotor, rad} \cdot \text{s}^{-1} \end{aligned}$$

Introduction

MICRO air vehicles (MAVs) are a rapidly emerging field of research and are envisioned to have a wide range of military and civilian applications. Since MAVs are small and compact systems, they offer several advantages such as portability, rapid deployment, real-time data-acquisition capability, low radar cross section, low noise signatures, and low production costs. However, even though the concept of MAVs appears attractive, the MAV research is still in its incipient stages. The present status of MAVs is far from being viable for any challenging practical applications. However, it should be noted that only a decade of research has gone into these small vehicles and the key technical barriers are only being resolved now. Some of these barriers include efficient small-scale power generation and storage, out-of-sight navigation and communications, low-Reynolds-number aerodynamics, and autonomous control. One of the most important and least understood aspects of small-scale flight is its aerodynamic performance.

From an aerodynamics perspective, the key challenge for an MAV designer is the low lift-to-drag ratios (L/Ds) of even the most optimized airfoil geometries at low Reynolds numbers. Several fixed-wing MAVs have already been successfully tested [1–5]. One particular example [4,5] has a weight of 80 g and a flight endurance of about 30 min. Even though fixed-wing MAVs may be the best performers today with the imposed size and weight constraints, they lack the ability to hover or to operate in confined environments. These latter attributes are important for many missions, including surveillance in constrained areas such as building interiors, caves, and tunnels. Therefore, the development of efficient hovering concepts will lead to more versatile MAVs with expanded flight envelopes. At present, rotary wings are the most practical choice for hovering and low-speed flight. To this end, several hover-capable MAVs based on single main rotor or coaxial rotor configurations have been successfully built and flight tested [6–9]. However, hovering and low-speed flight modes are already states of high power consumption, and the situation is further exacerbated by the degraded performance of conventional airfoils at the low-Reynolds-number range (10,000–50,000) at which these MAVs operate. In fact, most MAVs based on conventional rotors have shown relatively low performance, e.g., the maximum figure of merit achieved to date is only about 0.65 [6,8]. This implies that scaling down full-scale

Received 6 April 2011; revision received 1 July 2012; accepted for publication 25 July 2012; published online 11 July 2013. Copyright © 2012 by the American Institute of Aeronautics and Astronautics, Inc. All rights reserved. Copies of this paper may be made for personal or internal use, on condition that the copier pay the \$10.00 per-copy fee to the Copyright Clearance Center, Inc., 222 Rosewood Drive, Danvers, MA 01923; include the code 1542-3868/13 and \$10.00 in correspondence with the CCC.

*Assistant Research Scientist, Department of Aerospace Engineering. Member AIAA.

†Graduate Research Assistant, Department of Aerospace Engineering. Student Member AIAA.

‡Alfred Gessow Professor and Director, Alfred Gessow Rotorcraft Center, Department of Aerospace Engineering. Fellow AIAA.

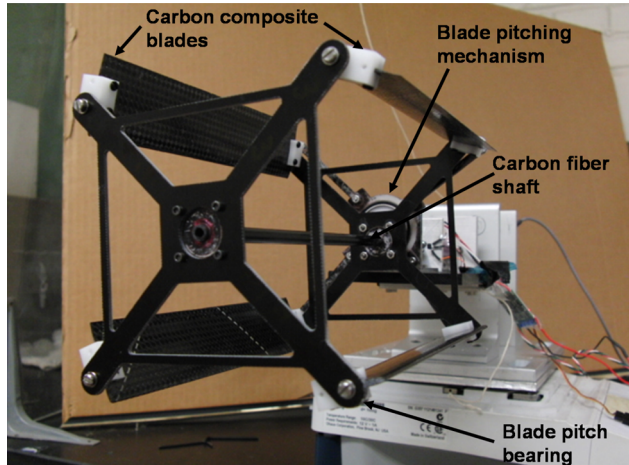


Fig. 1 Four-bladed cycloidal rotor with 3 in. radius, 6.25 in. blade span, and 1.33 in. blade chord (baseline rotor).

concepts such as fixed wings and helicopters may not be the right approach for operating in a completely different aerodynamic regime. Therefore, investigating alternate solutions such as cycloidal rotors, flapping wings, etc., is important because they might have potential for better performance at the low Reynolds numbers.

A MAV concept based on a cycloidal-rotor (cyclorotor) system instead of a conventional rotor has been proposed. A cyclorotor (also known as a cyclocopter or cyclogiro) is a rotating-wing system (Fig. 1) where the span of the blades runs parallel to the axis of its rotation. The pitch angle of each blade is varied cyclically by mechanical means such that the blade experiences positive angles of attack at both top and bottom halves of the azimuth cycle (Fig. 2). The resulting time-varying lift and drag forces produced by each blade are resolved into the vertical and horizontal directions, as shown in Fig. 2. Varying the amplitude and phase of the cyclic blade pitch is used to change the magnitude and direction of the net thrust vector produced by the cyclorotor.

Compared to a conventional rotor, each spanwise blade element of a cyclorotor operates at similar aerodynamic conditions (i.e., at same flow velocity, Reynolds number, and angle of incidence), and so the blades can be more easily optimized to achieve best aerodynamic efficiency. Moreover, because the blades are cyclically pitched once per revolution (1/rev), unsteady flow mechanisms may delay blade stall onset and in turn may augment the lift produced by the blades. Prior experiments have suggested that cyclorotors can reach efficiencies comparable to conventional rotor systems [10]. Further-

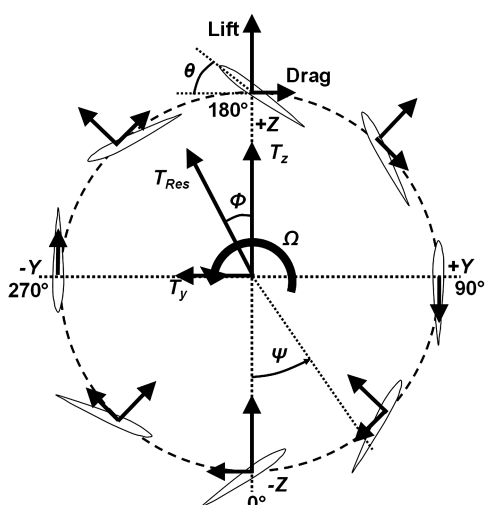


Fig. 2 Blade pitching kinematics and force vectors on a cyclorotor.

more, because the thrust vector of a cyclorotor can be almost instantaneously set to any direction perpendicular to the rotational axis, a cyclorotor-based MAV may ultimately show better maneuverability and agility as compared to a MAV powered by a conventional rotor system, which is a particularly important attribute for constrained indoor flight operations. One major drawback of a cyclorotor is its relatively large rotating structure, which might incur a weight penalty compared to a conventional rotor.

Even though the concept of cyclorotors has been around for almost a century [11], there have not been many systematic studies performed on this concept. Most of the studies that have been performed are mostly at relatively large scales ($Re > 100,000$) [11–24]. The key conclusions from these studies are summarized in [11,25]. One of the most challenging tasks with any hover-capable MAV design is to increase the flight endurance of the vehicle. To this end, the achievement of a high power loading (thrust per unit power) is a key factor in determining hovering flight efficiency. None of the previous studies carried out a comprehensive experimental parametric study to improve the performance of a cyclorotor at MAV-scale Reynolds numbers. Therefore, a primary goal of the present work was to carefully investigate the performance of the cyclorotor concept and to examine whether its hovering efficiency could be greater than that of a conventional rotor at the microscale.

Previous studies performed at the University of Maryland [10,25–29] included systematic experimental parametric studies on a microscale cyclorotor (diameter and span equal to 6 in.) by varying the rotational speed, blade airfoil profile, blade flexibility, blade pitching amplitude (symmetric and asymmetric blade pitching), pitching axis location, number of blades with constant chord (varying solidity), and number of blades at same rotor solidity (varying blade chord). Detailed particle image velocimetry (PIV) measurements were also performed to understand the flowfield of the cyclorotor. Significant improvement in the cyclorotor performance was achieved through these parametric studies, and the final efficiency of the cyclorotor was found to be comparable to that of a conventional microrotor at the same scale. A twin cyclocopter (weighing 215 g) capable of stable hover was also built to demonstrate the flightworthiness of the cyclorotor concept (Figs. 3 and 4) [29].

The present work is a continuation of this work reported in [10,25–29], and it is focused on achieving improvements in cyclorotor performance by varying the rotor geometry, which includes the rotor radius, blade span, chord, and blade planform. These parameters, when systematically varied, identified substantial improvements in performance. Once the optimized cyclorotor geometry was obtained, further improvements in performance were achieved by varying the blade kinematic parameters, such as amplitude of blade pitch (symmetric and asymmetric pitching) and chordwise blade pitching axis location. The final performance of the optimized cyclorotor is compared to that of a conventional rotor of the same scale.

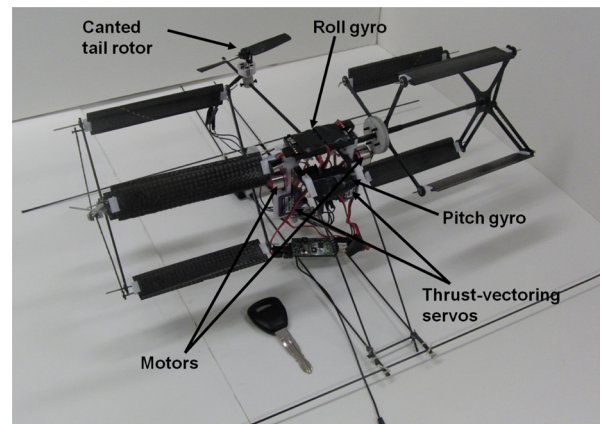


Fig. 3 215 g twin-rotor cyclocopter MAV.

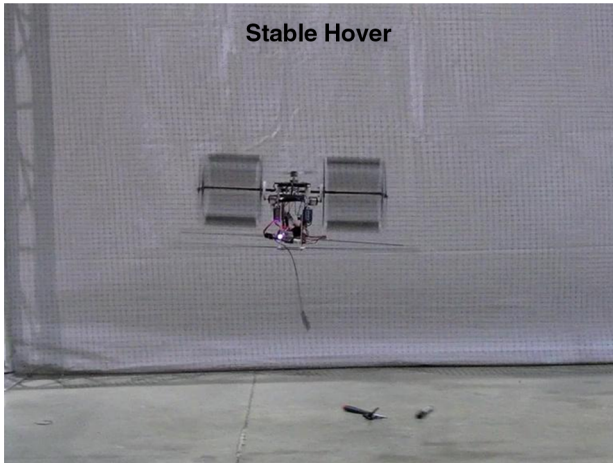


Fig. 4 Stable controlled hover of twin-cyclocopter.

Experimental Measurements

Several experiments were conducted on a MAV-scale cyclorotor (Fig. 1) to investigate the effects of rotor geometry and blade kinematics on performance in terms of both thrust and power loading (thrust/power). The rotor geometry parameters that were varied include the rotor radius R , blade span b , chord c , and blade planform. The blade kinematic parameters include rotational speed (revolutions per minute), amplitude of blade pitch (symmetric and asymmetric pitching), and chordwise blade pitching axis location. For the baseline cyclorotor, at the maximum rotational speed of 1800 rpm, the operating Reynolds number was 32,000.

A test setup with load cells was designed and built to measure the thrust, torque, and rotational speed of the cyclorotor. The baseline rotor had a diameter D of 6 in., blade span (b) of 6.25 in. (Fig. 1) and used four NACA 0015 blades with a chord of 1.33 in. A Hall-effect sensor was used to generate a 1/rev signal to measure the rotational speed. The power consumption was determined from the torque and rotational speed measurements. Details on the design of the cyclorotor and the blade pitching mechanism are provided in [25].

Measurements were taken on cyclorotors with different rotor geometry (radius, span, chord, and planform) and blade kinematics (rpm, pitching amplitude, and pitching axis location). The different rotor radii that were tested include 2, 3, 4, and 5 in. Four different blade spans, 3.75, 4.69, 6.25, and 9.38 in., were also studied. Various

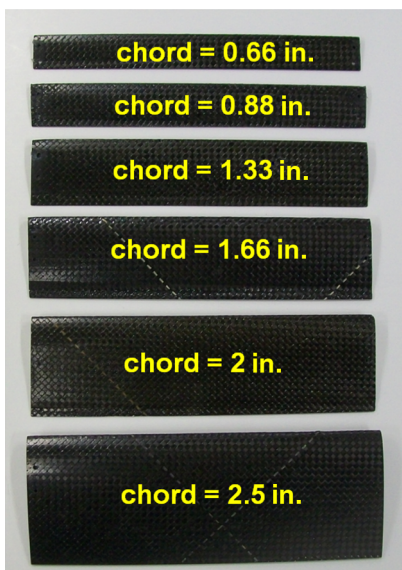


Fig. 5 Various blades tested with different chords and NACA 0015 airfoil section.

blade chords that were tested include 0.665, 0.887, 1.33, 1.665, 2.0, and 2.5 in. (Fig. 5). The different blade planforms studied include a rectangular blade and two trapezoidal blades with taper ratios of 1.75 and 2.25. All the blades used in this study had NACA 0015 airfoil section, except for the blade planform tests, which used flat plate blades.

As far as the blade kinematics is concerned, blade pitching amplitudes of 25°, 35°, 40° and 45°, were investigated for rotational speeds ranging from 400 to 1800 rpm. Various asymmetric pitching cases, where the blade attains different pitch angles at the top and bottom points of its trajectory, were also investigated for a blade peak-to-peak pitch angle of 70°. All the tests were performed using the pitching axis at 25% chordwise location except for the pitching axis variation tests and blade planform tests. Tests were also performed to determine the effect of chordwise pitching axis location by varying the pitching axis from 25% to 45% chord.

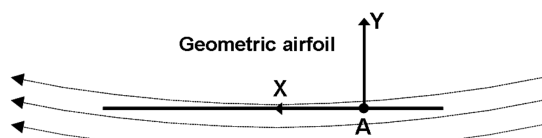
Results

The coordinate system used for the cyclorotor is shown in Fig. 2. The azimuthal position of the blade, Ψ , was measured counter clockwise from the negative Z-axis. The blade pitch angle, θ , was measured with respect to the tangent to the circular path of the blade. Figure 2 shows the schematic of the forces produced by the cyclorotor. Intuitively, it might be expected that a cyclorotor should only produce a vertical force, T_z . However, subsequent tests clearly showed that the cyclorotor also produced a significant sideward force, T_y , whose magnitude was comparable to that of the vertical force (Fig. 2). In the remainder of the paper, the thrust refers to the resultant thrust (i.e., to T_{Res}).

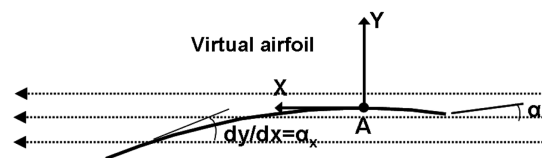
The total aerodynamic power includes the induced power, the profile power, the rotational flow losses, the aerodynamic power required for cyclically pitching the blades, and the profile power associated with moving the structure of the cyclorotor (other than the blades). Tare tests were carried out at different rotational speeds after removing the blades to measure the parasitic profile power associated with the structure. These measurements were then subtracted from the total power measurements to obtain the aerodynamic power required to rotate the blades. Tare losses were found to constitute about 10–15% of the total aerodynamic power.

Flow Curvature Effects (Virtual Camber and Incidence Effects)

The virtual camber/incidence effects due to the flow curvature needs to be introduced in order to explain most of the results in the present study. Virtual camber effect is an aerodynamic phenomenon commonly found in vertical axis wind turbine blades where the blades undergo an orbital motion and therefore experience a curvilinear flow. Blades subjected to a curvilinear flow behave very differently compared to being immersed in a rectilinear flow (Fig. 6). In a curvilinear flow, the local velocity and angle of attack of the blade are unique at different locations along the chord. Because of this, a symmetric blade at 0° pitch angle in a curvilinear flow (Fig. 6a) can be



a) Curvilinear flow with straight airfoil



b) Rectilinear flow with cambered airfoil

Fig. 6 Virtual camber in a curvilinear flow.

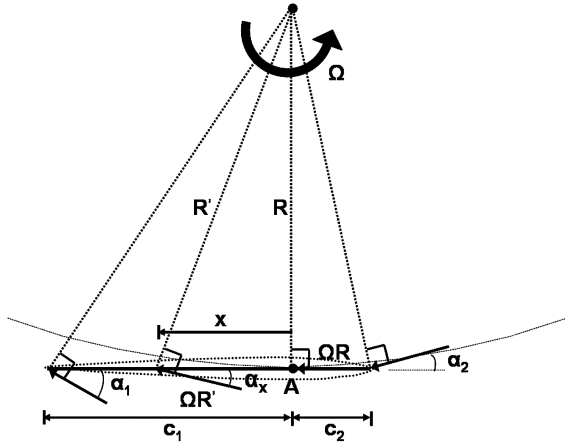


Fig. 7 Schematic explaining virtual camber.

viewed to behave like a cambered blade at an angle of incidence (α_i) in a rectilinear flow (Fig. 6b). This effect will be more pronounced with cyclorotors having large chord-to-radius ratio (c/R).

The virtual camber effect is clearly explained using Fig. 7, which shows a symmetric airfoil at a pitch angle of 0° at the bottom most point of the blade trajectory. Point A is the pitching axis of the blade. For the sake of explanation, resultant velocity at any location on the blade chord is assumed a function of the rotational speed only (the induced velocity and the pitch rate effects are ignored). Thus, as shown in Fig. 7, the magnitude and direction of the resultant velocity varies along the chord. The angle of incidence of the flow at any arbitrary location on the chord, x , is given by $\alpha_x = \tan^{-1}(x/R)$ ($\alpha_x \approx x/R$) and the velocity magnitude is given by $\Omega R'$ where $R' = \sqrt{R^2 + x^2}$.

Now this scenario is approximately equivalent to having a cambered airfoil, with the camber line slope (dy/dx) equal to α_x in a rectilinear flow of magnitude $\Omega R'$ as shown in Fig. 6b. Figure 8 shows the variation of virtual camber at different azimuthal locations for a flat plate blade pivoted at quarter chord but with no pitching. Because of the large chord/radius ratio of the cyclorotors investigated in the present study, there is significant virtual camber/incidence that is positive for the entire lower half and negative for the upper half. For the present baseline rotor (radius = 3", chord = 1.33", $c/R = 0.43$), the virtual camber is about 5.3% of chord and the virtual incidence is about 6.1° . However for some of the rotors that were tested, the chord/radius ratio was as high as 1.25 (radius = 2", chord = 2.5"). Virtual camber effect is directly dependent on the chord/radius ratio of the cyclorotor and should play a significant role in the aerodynamic performance of such rotors.

For a moderate flow curvature and for attached flow, the influence of virtual camber/incidence on the aerodynamic coefficients can be

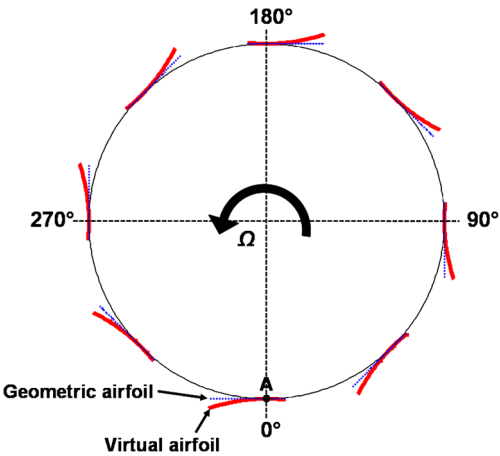


Fig. 8 Virtual camber at different azimuthal location for a blade pivoted at a quarter-chord and no pitching.

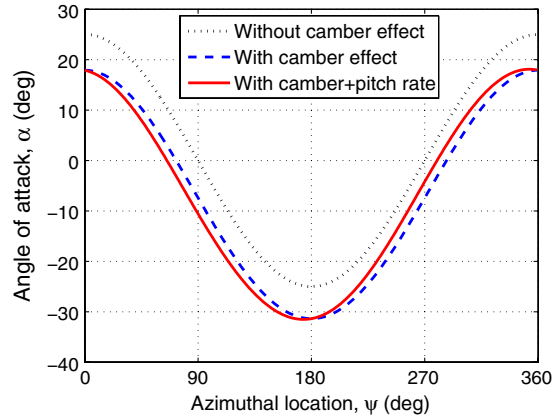
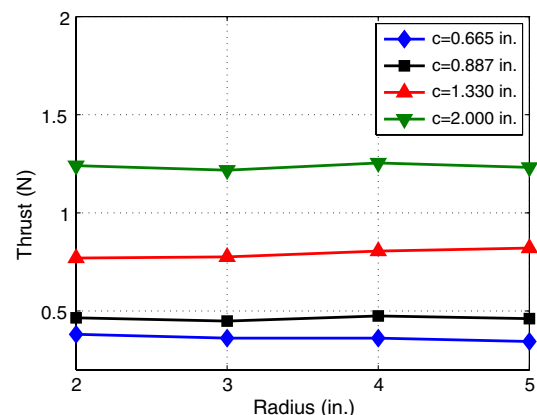


Fig. 9 Effect of virtual camber and pitch rate on the effective angle of attack.

accommodated by a shift in angle of attack [30,31]. Using thin airfoil theory, the strength of the circulation of a camber line with constant curvature is such that the flow at the $3/4$ chord location is in the direction of the camber line. Hence, the angle of attack in the curved flow is evaluated with the flow curvature at the $3/4$ chord location [32]. In the subsequent sections, the influence of virtual camber on lift is taken into account by calculating the angle of attack at the $3/4$ chord location. The effect of flow curvature on drag coefficient can be introduced as a correction in zero-lift drag coefficient (C_{d_0}) [33]. Figure 9 shows the effect of virtual camber and pitch rate on the effective angle of attack variation at the $3/4$ chord location (without the effect of inflow) of a cyclorotor blade for a pitching amplitude of 25° . With the addition of virtual camber, there is a significant shift in the angle of attack at the $3/4$ chord, which can be viewed as a decrease in the effective angle of attack at the upper half and increase in the angle of attack at the lower half of the circular blade trajectory. Because of this, asymmetric blade pitching and the pitching axis location can affect the performance of a cyclorotor. The flow curvature effects may also improve the performance of the rotor to some extent and there can be an optimum chord/radius ratio for the cyclorotor. Investigating this aspect is one of the key objectives of the present study.

Effect of Rotor Radius

Rotors with four different radii, 2, 3, 4, and 5 in., were tested at fixed blade chords to investigate the effect of rotor radius (or chord/radius ratio) on the performance of the cyclorotor in terms of thrust and power loading (thrust/power). Figure 10 shows the variation of resultant thrust with rotor radius at a constant blade speed of 9.58 m/s (at the blade pitching axis) for different blade chords at a pitching amplitude of 40° . For obtaining a blade translational speed

Fig. 10 Thrust versus rotor radius for the cyclorotor using blades with different chords c at a 40° pitching amplitude at a constant blade speed of 9.58 m/s.

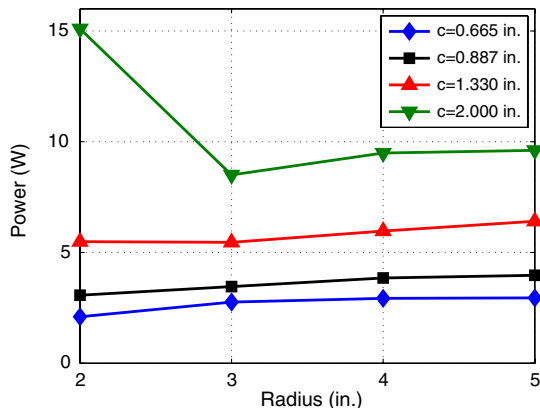


Fig. 11 Power versus rotor radius for the cyclorotor using blades with different chords c at a 40 deg pitching amplitude at a constant blade speed of 9.58 m/s.

of 9.58 m/s, the corresponding rotational speeds for 2, 3, 4, and 5 in. radius rotors are 1800, 1200, 900, and 720 rpm, respectively. If the flow curvature effects (virtual camber/incidence) are not taken into account, the thrust and power are not expected to vary with radius since the blade speed is constant. From Fig. 10, it can be seen that the thrust does not vary much with radius (or chord/radius ratio) for the different blade chords tested. This shows that the time-averaged thrust is not significantly affected by the flow curvature effects. On the other hand, as shown in Fig. 11, for a constant blade speed, power varies significantly with radius, especially for the larger chords. Now, since power strongly depends on the flow curvature effects, the power loading (thrust/power) of the cyclorotor would vary significantly with radius (for a constant chord).

Figures 12–15 show the variation of power loading with disk loading (thrust per unit actuator area) at different rotor radii for four different blade chords at a pitching amplitude of 40°. The actuator area used for calculating the disk loading of the cyclorotor is the rectangular projected area of rotor, (span × diameter). In the rest of the paper, all the different test cases will be compared using power loading versus disk loading since they provide a good measure of the efficiency of the cyclorotor.

Figure 12 shows the variation of power loading with disk loading for 2, 3, 4, and 5-in.-radius rotors using blades with 1.33 in. chord. As shown in the figure, maximum power loading was obtained for the 2-in.-radius rotor followed by 3, 4, and 5 in. radii. The chord/radius ratios for the 2, 3, 4 and 5 in. rotors are 0.665, 0.443, 0.332, and 0.266, respectively. These results clearly show that the performance improves as the chord/radius ratio of the rotor was increased from 0.266 to 0.665. However, based on these results, the optimum chord/radius can be even higher than 0.665.

For the rotors with 1.67 in. blade chord (Fig. 13), the trend remained the same with 2 in. radius producing the maximum power

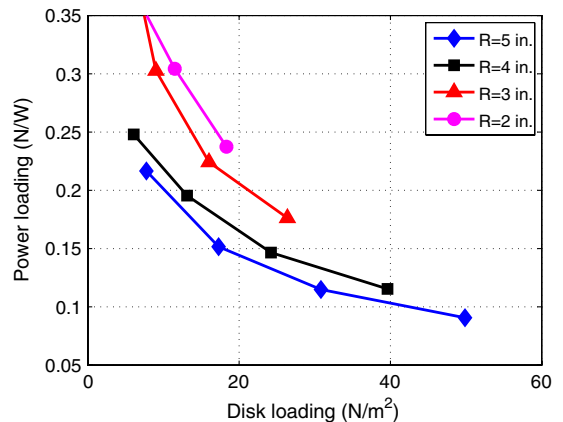


Fig. 13 Power loading versus disk loading for the cyclorotor using 1.665-in.-chord blades for different rotor radii R at a 40 deg pitching amplitude.

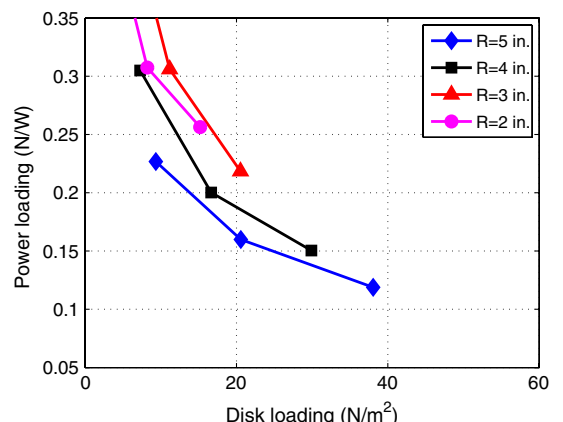


Fig. 14 Power loading versus disk loading for the cyclorotor using 2-in.-chord blades for different rotor radii R at a 40 deg pitching amplitude.

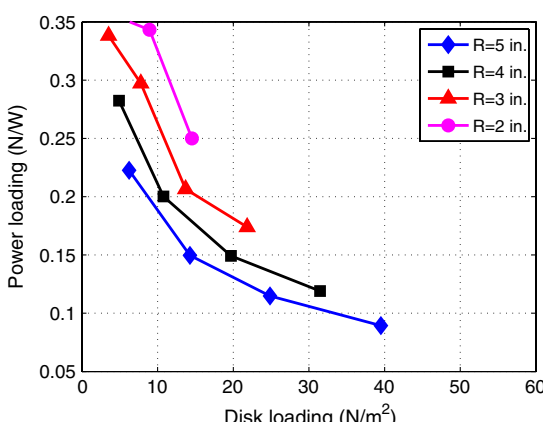


Fig. 12 Power loading versus disk loading for the cyclorotor using 1.33-in.-chord blades for different rotor radii R at a 40 deg pitching amplitude.

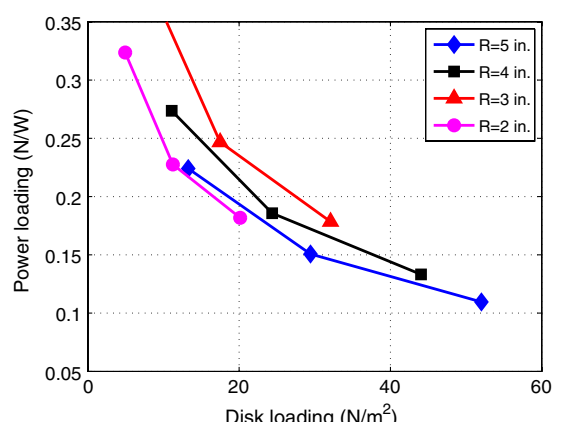


Fig. 15 Power loading versus disk loading for the cyclorotor using 2.5-in.-chord blades for different rotor radii R at a 40 deg pitching amplitude.

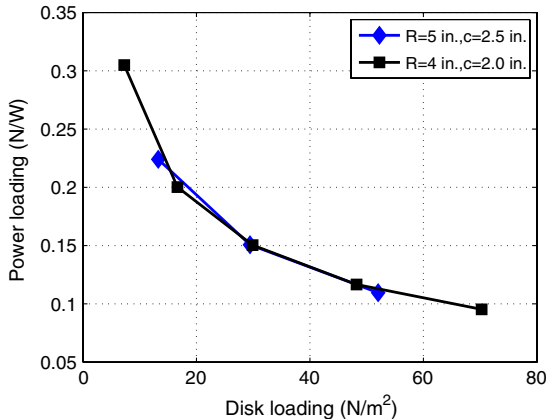


Fig. 16 Power loading versus disk loading for cyclorotors with two different rotor radii but at the same chord/radius ratio ($c/R = 0.5$) at a 40 deg pitching amplitude.

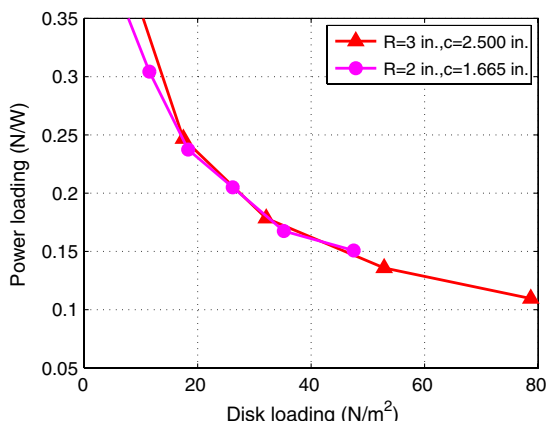


Fig. 17 Power loading versus disk loading for cyclorotors with two different rotor radii but at the same chord/radius ratio ($c/R = 0.83$) at a 40 deg pitching amplitude.

corresponds to a c/R of 1.25 which is even worse than the 5 in. rotor which has a c/R of 0.5.

In all the above results there are two parameters varying, the radius and the chord/radius ratio. It is important to understand whether these differences in performance can be attributed to the chord/radius ratio or to the radius itself. Therefore, to understand this, rotors with different radii, but with the same chord/radius ratio were compared in Figs. 16–19. Figures 16 and 17 show the variation of power loading with disk loading for chord/radius ratios of 0.5 and 0.83, respectively, at 40° pitching amplitude. Whereas, Figs. 18 and 19 show the

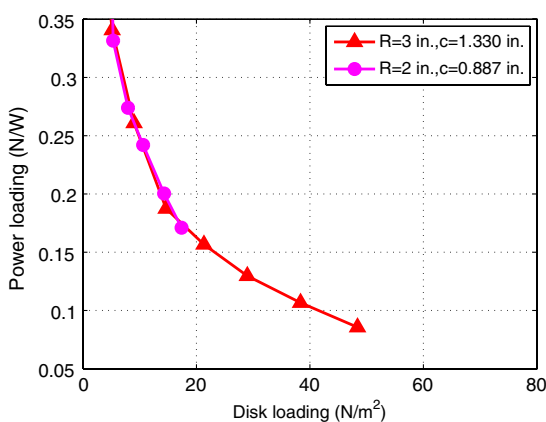


Fig. 18 Power loading versus disk loading for cyclorotors with two different rotor radii but at the same chord/radius ratio ($c/R = 0.44$) at a 25 deg pitching amplitude.

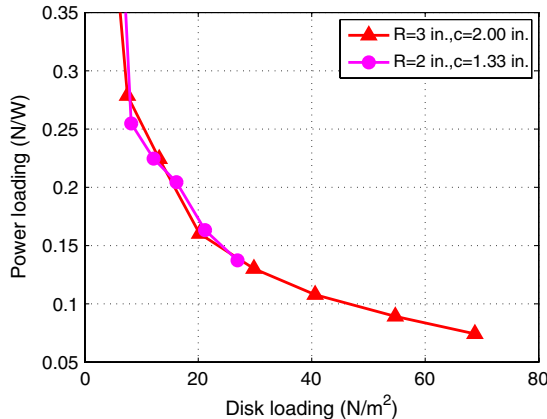


Fig. 19 Power loading versus disk loading for cyclorotors with two different rotor radii but at the same chord/radius ratio ($c/R = 0.66$) at a 25 deg pitching amplitude.

variation of power loading at 25° pitching amplitude for chord/radius ratios of 0.44 and 0.66, respectively. These results clearly show that the power loading is identical as long as the chord/radius ratios are the same even if the radii of the rotors are different.

Having shown that, for a constant disk loading, the power loading is only dependent on chord/radius ratio, all the above results for different radii and blade chords can be combined to obtain the variation of power loading with chord/radius ratio. Figures 20 and 21 show the variation of power loading with chord/radius ratio at constant disk loadings for 40° and 25° pitching amplitudes, respectively. The varying radius tests were performed at 25° pitching amplitude also because, since the finite chord introduces a virtual camber and incidence on the cyclorotor blades, the optimum chord/radius ratio should also depend on the pitching amplitude of the blades. As shown in Fig. 20, at 40° pitch amplitude, for all the three disk loadings, the power loading increases with chord/radius, reaching the optimum at around 0.83 and drops drastically as the chord/radius is increased further. However, in the case of 25° pitching amplitude (Fig. 21), the optimum chord/radius ratio is around 0.5. However, as the chord/radius is increased further up to 1.25, the drop in power loading is not as drastic as the 40° pitching amplitude case.

Following are the key conclusions from the above results. The power loading of the cyclorotor is strongly dependent on the chord/radius ratio and not the radius itself (for a constant disk loading). The study also showed that the cyclorotor achieves higher power loading values at higher chord/radius ratios. It was also significant to see that the optimum chord/radius ratio is a function of the pitching amplitude. The best chord/radius ratios for 40° and 25° pitching amplitudes were around 0.8 and 0.5, respectively. The strong dependency of the cyclorotor performance on the chord/radius ratio can be attributed to the flow curvature effects (virtual camber and

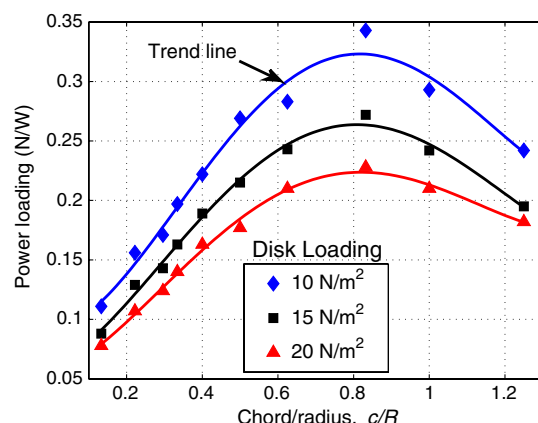


Fig. 20 Power loading versus chord/radius at constant disk loading at a 40 deg pitching amplitude.

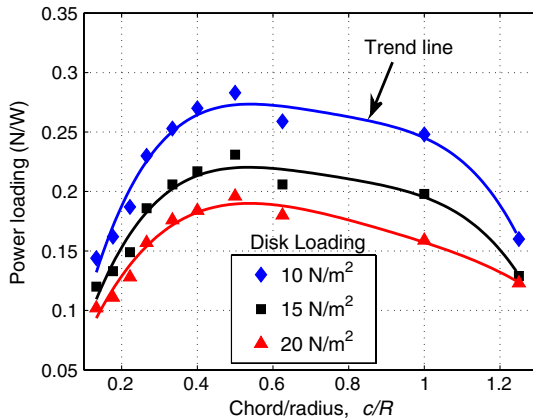


Fig. 21 Power loading versus chord/radius at constant disk loading at a 25 deg pitching amplitude.

incidence) explained in the previous section. For a chord/radius of 0.8, the virtual camber and incidence can be as high as 9.5% and 11°, respectively.

Effect of Blade Span

Cyclorotors with four different blade spans (3.75, 4.69, 6.25 and 9.38 in.) were tested at the same radius (3 in.), chord (1.33 in.) and blade kinematics to understand the effect of rotor span on the performance of the cyclorotor. Figure 22 shows the variation of the thrust produced per unit span of the rotor with blade span at a pitching amplitude of 25°. It is significant to note that the thrust producing capability of the rotor per unit span decreases linearly with blade span for a constant rotational speed. On the other hand, as shown in Fig. 23, the power required per unit span increases linearly from a blade span of 3.75 in. to 6.25 in.; however, the increase from 6.25 in. to 9.38 in. is significantly small.

Figure 24 shows the variation of power loading with disk loading for the same case. As expected from the trends in thrust and power, the power loading steadily decreases as the blade span was increased from 3.75 to 9.38 in. However, for the 40° pitching amplitude case (Fig. 25), unlike the 25° case, the power loadings for all the blade spans were similar, even though the rotors with the shorter span performed slightly better at higher disk loadings. The reason for the shorter span blades performing better than the longer ones is not completely understood at this point.

Effect of Rotor Aspect Ratio (Span/Diameter)

In the previous two sections, the effect of chord/radius ratio and blade span were independently investigated. It was shown that, for each pitching amplitude, there is an optimum chord/radius ratio. The blade span studies showed that the blades with shorter span perform

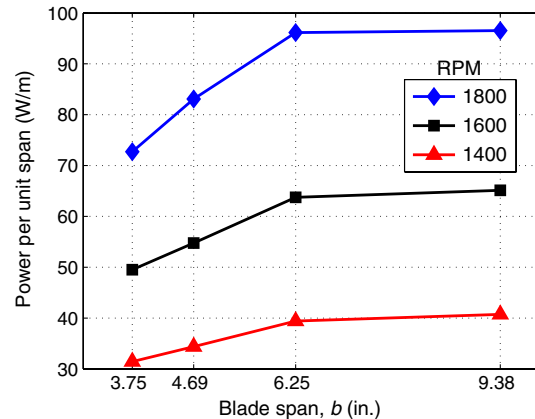


Fig. 23 Power per unit span versus blade span at constant rotational speed for the 3-in.-radius 1.33 in. blade chord cyclorotor at a 25 deg pitching amplitude.

better for the same disk loading, especially at lower pitching amplitudes (25°). Therefore, the goal of this study was to combine these two effects and obtain the optimum aspect ratio (span/diameter or b/D) for the cyclorotor for a fixed blade chord (1.33 in.). The different aspect ratios were chosen such that the rectangular projected area of the rotor (span × diameter) was the same for all the cases. The different radius and blade span combinations that were tested include, $R = 5$ in. and $b = 3.75$ in. ($AR = 0.38$), $R = 4$ in. and $b = 4.69$ in. ($AR = 0.59$), $R = 3$ in. and $b = 6.25$ in. ($AR = 1.04$), and

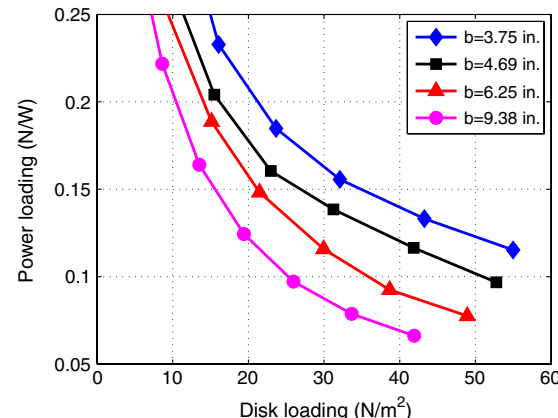


Fig. 24 Power loading versus disk loading for the 3-in.-radius 1.33 in. blade chord cyclorotor for different blade spans b at a 25 deg pitching amplitude.

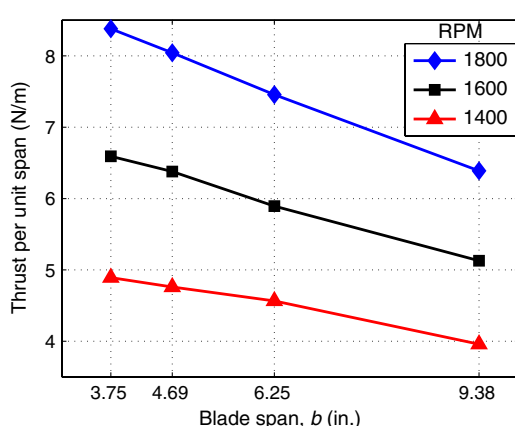


Fig. 22 Thrust per unit span versus blade span at constant rotational speed for the 3-in.-radius 1.33 in. blade chord cyclorotor at a 25 deg pitching amplitude.

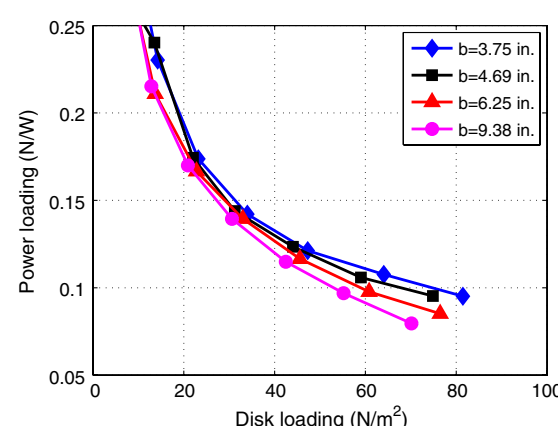


Fig. 25 Power loading versus disk loading for the 3-in.-radius 1.33 in. blade chord cyclorotor for different blade spans b at a 40 deg pitching amplitude.

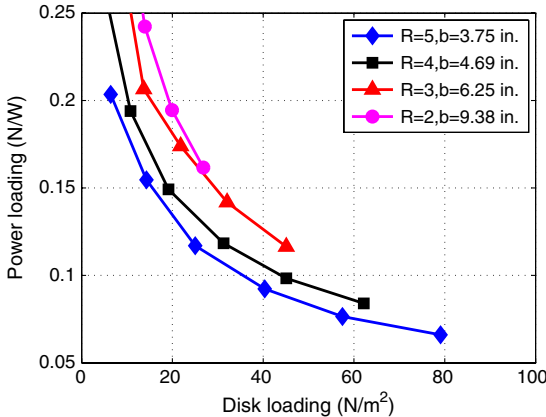


Fig. 26 Power loading versus disk loading for different rotor aspect ratios (b/D) at a 40 deg pitching amplitude.

$R = 2$ in. and $b = 9.38$ in. ($AR = 2.34$). All these rotors had a projected area of 37.5 square in., so that the ideal induced power can be assumed to be the same for all the rotors. The tests were performed at pitching amplitudes of 25° , and 40° .

Figure 26 shows the variation of power loading with disk loading for the different aspect ratio rotors at 40° pitching amplitude. The results clearly show that the power loading increased with increasing aspect ratio and the rotor with 2 in. radius and 9.38 in. span has the highest power loading indicating that a higher aspect ratio is better for a cyclorotor. However, before coming to such a conclusion, it is important to break down the effect of aspect ratio into the blade span effect and the chord/radius ratio effect. As seen from the blade span studies in Fig. 25, for the 40° pitching amplitude, the blade span did not have a significant impact on the power loading at the same disk loading. Therefore, for the 40° pitching amplitude, the blade span effect can be ignored and the aspect ratio effect can be explained purely based on the chord/radius ratio effect. It has been shown in the previous section that the power loading of the cyclorotor increases with chord/radius ratio until a c/R of 0.8 for the 40° pitching amplitude. For the rotors used in the aspect ratio study the chord/radius ratio varied from 0.27 ($R = 5''$) to 0.66 ($R = 2''$). Therefore, in this case, the improvement in performance from 5 in. radius to 2 in. radius can be because the rotor is operating at a better chord/radius ratio. Also, Fig. 12 (varying radius tests) clearly shows that the optimum radius for a rotor using 1.33 in. blade chord is 2 in.

However as shown in Fig. 27, the 25° pitching amplitude case showed a trend opposite to the 40° case. The power loading now improved as aspect ratio was decreased from 2.34 ($R = 2''$ and $b = 9.38''$) to 0.59 ($R = 4''$ and $b = 4.69''$). From 0.59 to 0.38 ($R = 5''$ and $b = 3.75''$), the power loading dropped. Again as in the previous case, the aspect ratio effect can be broken down into the span effect and chord/radius ratio effect. Based on the blade span

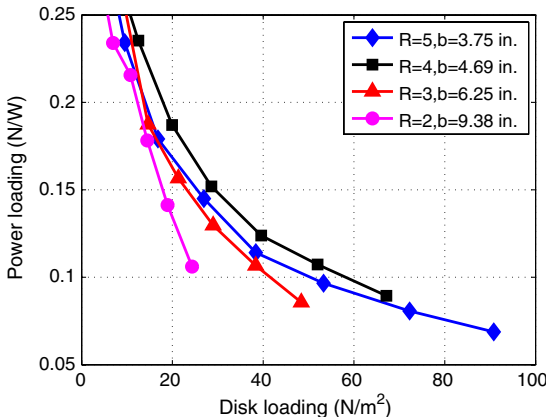


Fig. 27 Power loading versus disk loading for different rotor aspect ratios (b/D) at a 25 deg pitching amplitude.

studies, unlike the 40° case, for the 25° pitching amplitude, there was a significant improvement in power loading as the blade span was decreased (Fig. 25). Purely based on the span effect, the optimum should have been 5 in. radius and 3.75 in. span. And only based on chord/radius ratio, the best case should have been 3 in. radius and 6.25 in. span because the optimum c/R at 25° was around 0.5. However, because of a combination of these two effects, the optimum for the 25° pitching amplitude occurred at 4 in. radius and 4.69 in. blade span. These studies clearly show that it is important to choose the right combination of blade span and chord/radius ratio in order to maximize the efficiency of the cyclorotor.

Effect of Rotor Solidity

There are two ways of increasing the solidity of any rotor. One way is to increase the number of blades keeping the blade chord constant and the other method is to increase the blade chord while retaining the same number of blades. For a conventional rotor, either of these options would produce comparable results. However, for a cyclorotor, the two methods arrive at completely different results. If the first method is followed, the solidity of the cyclorotor ($\sigma = N_b c / 2\pi R$) can be increased without changing the chord/radius ratio of the rotor. However, in the second option, since the blade chord is changed for a fixed rotor radius, both the solidity and the chord/radius ratio of the cyclorotor is changed. In the previous section it has been clearly shown that because of the flow curvature effects the performance of the rotor is a strong function of the chord/radius ratio.

The first method, where the solidity is increased by increasing the number of blades, has been previously investigated in [26]. For all the pitching amplitudes that were investigated in this study, the power loading increased until a solidity of 0.25. This is because of the fact that a rotor with higher solidity can achieve a given value of thrust at a lower rotational speed compared to a rotor with a lower solidity. The associated reduction in the profile power due to the lower operating rpm outweighs the increase in profile power due to the increased blade area. However, beyond a certain solidity, there was no improvement because the interference effects will tend to dominate. The main objective of the study in [26] was to take advantage of the increased total blade area in improving the power loading of the cyclorotor.

However, in the present study, the second option is investigated because as the chord is increased for a fixed radius, both the total blade area and the chord/radius ratio increases; and the results from the previous sections clearly show that the cyclorotor performs better at higher chord/radius ratios. Therefore, the goal of the present study is to take advantage of both the increased blade area and the higher chord/radius ratio of the rotor to improve the power loading.

In order to vary the rotor solidity for a fixed number of blades, five NACA 0015 blades with different blade chord ranging from 0.887 to 2.5 in. were fabricated (Fig. 5). The tests were performed at three different rotor radii (2, 3 and 4 in.) at 25 and 40 deg pitching

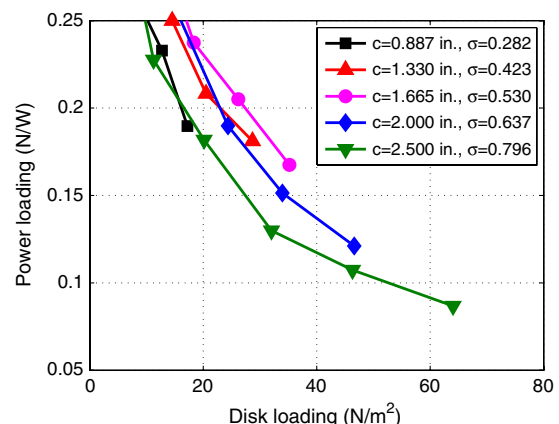


Fig. 28 Power loading versus disk loading for 2-in.-radius cyclorotor using different blade chords (rotor solidity, σ) at a 40 deg pitching amplitude.

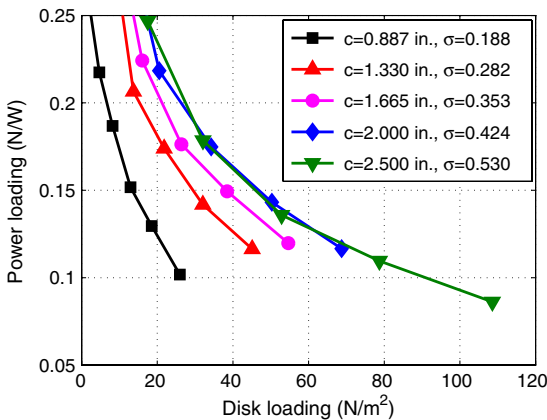


Fig. 29 Power loading versus disk loading for 3-in.-radius cyclorotor using different blade chords (rotor solidity, σ) at a 40 deg pitching amplitude.

amplitudes. Figure 28 shows the variation of power loading with disk loading for a 2-in.-radius rotor at 40 deg pitching amplitude. As shown in the figure, the power loading of the rotor increased with rotor solidity up to $\sigma = 0.53$, which corresponds to a c/R of 0.83 (chord = 1.665 in.), and thereafter a further increase in solidity lowered the power loading. Again, for the 3-in.-radius rotor (Fig. 29), the power loading improved with solidity until $\sigma = 0.42$ (chord = 2 in., $c/R = 0.67$). However, from $\sigma = 0.42$ to $\sigma = 0.53$ (chord = 2.5 in., $c/R = 0.83$), there was hardly any improvement. Since, the solidity decreases with increasing radius for the same chord, the maximum solidity that could be achieved for a 4-in.-radius rotor was 0.4 (chord = 2.5 in., $c/R = 0.625$). For the 4-in.-radius case (Fig. 30), the power loading steadily increased until 2.5 in. chord. Therefore, for the 4 in. rotor, there is scope of improvement if the solidity is increased further.

It is interesting to note that, in all the preceding results, the optimum solidity corresponds to a chord/radius of 0.7–0.8, which was in fact the optimum chord/radius ratio for a 40 deg pitching amplitude (Fig. 20). However, it is not necessary that the optimum solidity has to occur at the best chord/radius ratio, even though it is a significant factor. This is because of the fact that, along with the chord/radius ratio, the total blade area of the rotor is also varying, and it has been shown earlier [26] that the blade area has a significant impact on the power loading of the cyclorotor.

All the aforementioned tests were repeated for a 25 deg pitching amplitude because it was seen that the optimum chord/radius varies with pitching amplitude. Figures 31–33 show the variation of power loading with disk loading for 2-, 3-, and 4-in.-radius rotors at a 25 deg pitching amplitude. For the 2-in.-radius rotor (Fig. 31), the power loading improved when the solidity was increased from 0.28 (chord = 0.887, $c/R = 0.44$) to 0.42 (chord = 1.33, $c/R = 0.66$).

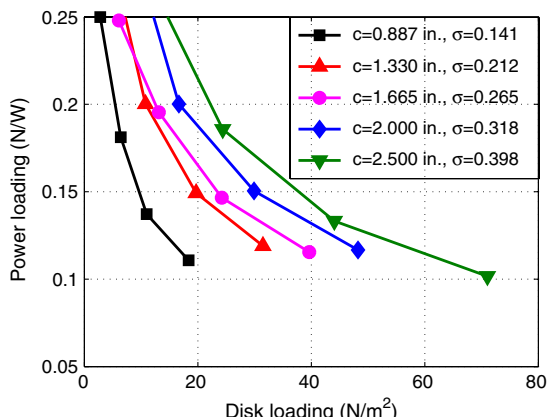


Fig. 30 Power loading versus disk loading for 4-in.-radius cyclorotor using different blade chords (rotor solidity, σ) at a 40 deg pitching amplitude.

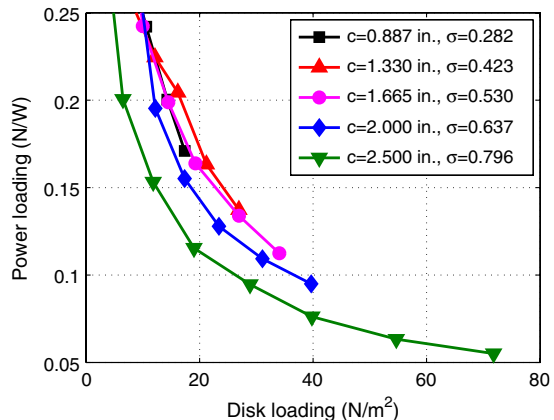


Fig. 31 Power loading versus disk loading for 2-in.-radius cyclorotor using different blade chords (rotor solidity, σ) at a 25 deg pitching amplitude.

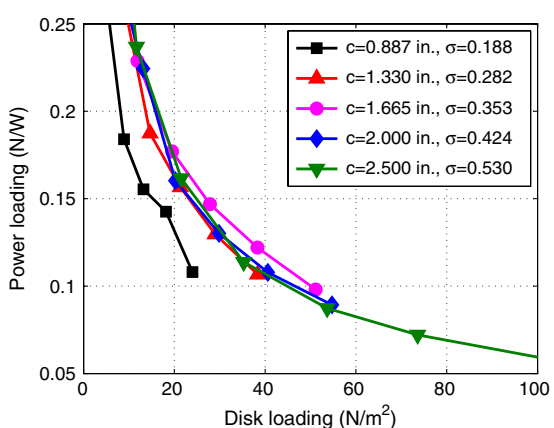


Fig. 32 Power loading versus disk loading for 3-in.-radius cyclorotor using different blade chords (rotor solidity, σ) at a 25 deg pitching amplitude.

However, beyond $\sigma = 0.42$, the power loading steadily dropped with the increase in solidity. However, for the 3-in.-radius rotor (Fig. 32), the power loading increased until a solidity of 0.35 (chord = 1.665, $c/R = 0.56$), beyond which it decreased. For the 2- and 3-in.-radius rotors, the optimum solidity corresponds to the best chord/radius ratio (0.5–0.6) for the 25 deg pitching amplitude case (Fig. 21). However, this is not true for the 4 in. rotor (Fig. 33), where the rotors with solidities of 0.26 (chord = 1.665, $c/R = 0.42$), 0.32 (chord = 2, $c/R = 0.5$), and 0.4 (chord = 2.5, $c/R = 0.62$) have very similar power loadings. This shows that, for a constant disk

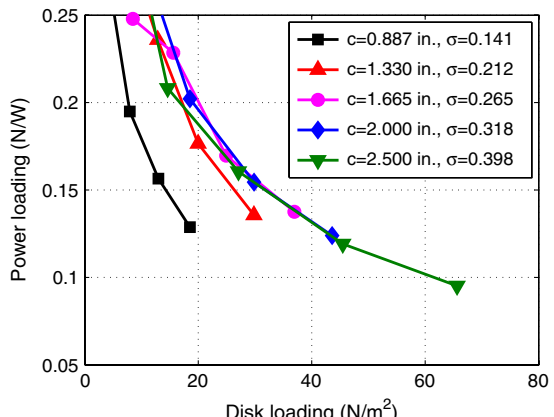


Fig. 33 Power loading versus disk loading for 4-in.-radius cyclorotor using different blade chords (rotor solidity, σ) at a 25 deg pitching amplitude.

loading, the maximum power loading not only depends on the optimum chord/radius ratio but also on the total blade area of the rotor.

One key conclusion from this study is that, if the solidity of the cyclorotor needs to be increased, the better approach is to increase the blade chord by keeping the number of blades fixed rather than increase the number of blades using a smaller blade chord. This way, the rotor can take advantage of both the increase in total blade area and higher chord/radius ratio. In this case, the optimum blade chord (or solidity) will be determined by the optimum chord/radius ratio for the operating pitching amplitude and the blade interference effects, which would start to dominate beyond a certain solidity.

Effect of Blade Planform

Because each blade of the cyclorotor has two free tips operating at the same velocity, a pair of counter-rotating tip vortices will be produced similar to that of a fixed wing. The PIV studies in [25] (Fig. 34) and the computational fluid dynamics simulation in [34] have clearly shown the presence of these tip vortices. Hence, changing the blade planform from rectangular to elliptical, or even trapezoidal, should improve the performance of the cyclorotor. Therefore, experiments were conducted on two trapezoidal blades (taper ratio = 1.75 and 2.25) and a rectangular blade (Fig. 35) to investigate the effect of blade planform on the performance of the cyclorotor. The taper ratio is defined as the ratio of midspan chord to the tip chord. All the three blades had the same area and aspect ratio

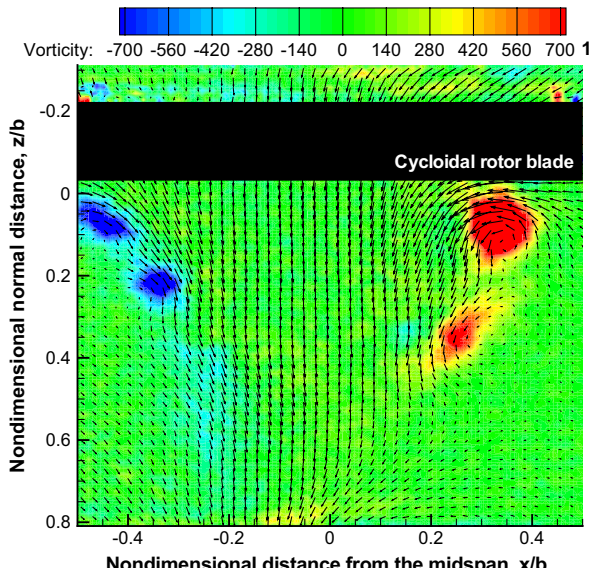


Fig. 34 Tip vortices on a cyclorotor blade operating at a 40 deg pitching amplitude [25].

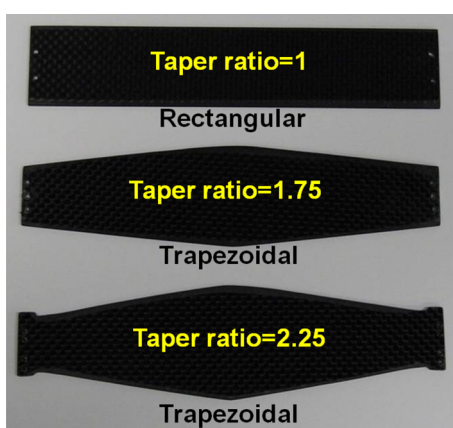


Fig. 35 Different blade planforms that were tested.

and used a flat-plate airfoil section with a 5% thickness-to-chord ratio (for the rectangular blade with 1.33 in. chord and 6.25 in. span) and sharpened leading and trailing edges. It should be noted that, for the trapezoidal blades, the chord/radius ratio varies along the blade span. However, since the blades have the same area, the average chord/radius ratios of all the blades are the same. Also, it is important to pitch all the blades at the 50% chordwise location so that the virtual incidence is zero.

The variation of power loading with disk loading for the rotors using different planform blades at 40 deg pitching amplitude is presented in Fig. 36. As expected, the trapezoidal blades with a taper ratio of 1.75 performed slightly better than the rectangular blades at higher disk loadings. However, when the taper ratio was increased to 2.25, the power loading dropped.

Based on the rotor geometry studies, the optimum rotor (highest power loading for the same disk loading) was a 3-in.-radius rotor with a blade span of 6.25 in. and chord of 2 in.

Effect of Blade Kinematics

Once the optimum rotor geometry was obtained, the next step was to vary the blade kinematics to further improve the performance of the cyclorotor. Previous studies [10,25,26] have shown that the blade kinematic parameters such as pitching amplitude, asymmetry in blade pitching (dissimilar pitch angles at the top and bottom halves), and pitching axis location have significant impact on the performance of the cyclorotor. Therefore, the optimum rotor geometry from the previous section was chosen and the aforementioned blade kinematic parameters were varied in the hope of further improving the performance of the cyclorotor.

Blade Pitching Amplitude (Symmetric Pitching)

Operating at the optimum cyclic pitching amplitude is important to maximize the power loading of the cyclorotor. Previous studies [10] have shown that operating at higher pitching amplitudes improves the performance of the cyclorotor. Therefore, the rotors were tested at blade pitching amplitudes of 35, 40, and 45 deg. In these tests, the blades were pitched symmetrically, which means the blade attains the same pitch angle at the top and bottom points ($\Psi = 180$ and 0 deg) of its circular trajectory. Figure 37 shows the variation of power loading with disk loading for the 3-in.-radius rotor using blades with a 2 in. chord and 6.25 in. span. This case was chosen because this was the optimum case from the rotor geometry studies in the previous sections. As shown in Fig. 37, the power loading improved from 35 to 40 deg pitching amplitudes and then dropped when the pitching amplitude was increased to 45 deg.

Higher power loading could be achieved at higher pitch angles because the power loading varies inversely with rotational speed; therefore, increasing thrust by increasing the blade section angle of attack seems more efficient than increasing the rotational speed. However, the maximum thrust that can be obtained using this

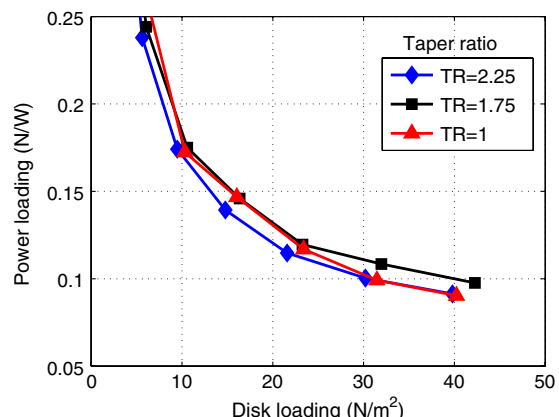


Fig. 36 Power loading versus disk loading for different blade planforms [taper ratios (TR)] at a 40 deg pitching amplitude and pitching axis at 50% chord location.

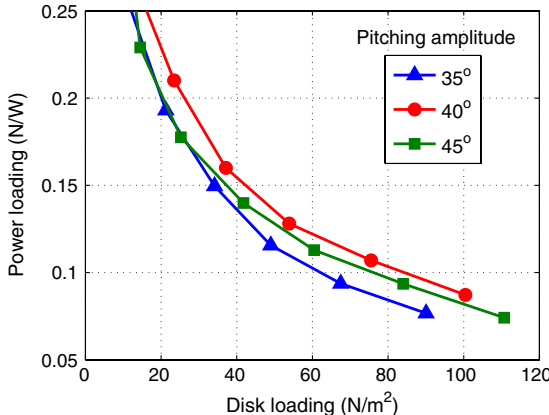


Fig. 37 Power loading versus disk loading for the 3-in.-radius rotor using 2-in.-chord 6.25-in.-span blades for three different pitching amplitudes with a pitching axis at a quarter-chord.

approach would still be limited by the onset of blade stall, and hence will be airfoil dependent. Also, at low Reynolds numbers, the profile drag coefficient is sensitive to the blade section angle of attack even before stall.

Asymmetric Blade Pitching

All the tests in the previous section were performed using a symmetric blade pitching, which means the blades have the same pitch angle at the top and bottom points of the blade trajectory. However, previous studies [10] have shown that this is not the optimum blade kinematics considering significant virtual camber/incidence effects, which reduces the lift at the top and increases the lift at the bottom (Fig. 8). The best power loading was obtained when the blades operated at a higher pitch angle at the top and a lower pitch angle at the bottom. Therefore, tests were conducted with dissimilar blade pitch angles at the top and bottom halves of the blade trajectory at a constant peak-to-peak pitch angle of 70 deg. Figure 38 shows the variation of power loading with disk loading for five different asymmetric cases for the 70 deg peak-to-peak pitch angle. The different cases were 30 deg at top and 40 deg at bottom (30°T, 40°B), 35 deg at top and bottom (35°T, 35°B), 40 deg at top and 30 deg at bottom (40°T, 30°B), 45 deg at top and 25 deg at bottom (45°T 25°B), and 50 deg at top and 20 deg at bottom (50°T 20°B). All these tests were conducted on a 3-in.-radius cyclorotor with a blade span of 6.25 in. and chord of 2 in.

Figure 38 shows that the lowest power loading was obtained for the 30 deg top/40 deg bottom case where the blades are operating at much higher pitch angle at the bottom compared to the top. However, as seen from Fig. 38, increasing the top angle and decreasing the bottom angle improved the power loading up to 45 deg top/25 deg bottom,

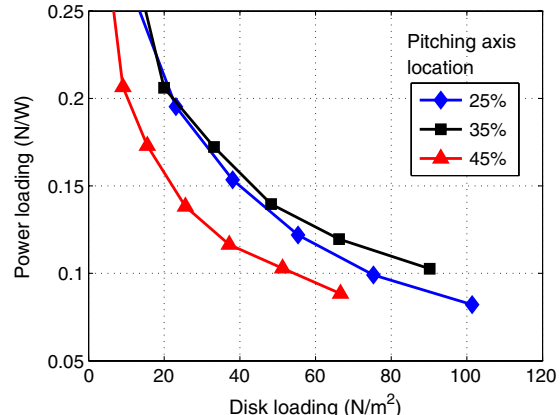


Fig. 39 Power loading versus disk loading for the 3-in.-radius rotor using 2-in.-chord 6.25-in.-span blades for three different pitching axis location at a pitching amplitude of 40 deg (symmetric pitching).

and then it decreased for the 50 deg top/20 deg bottom case, probably due to blades stalling at a 50 deg pitch angle. Therefore, the 45 deg top/25 deg bottom provided the optimum blade kinematics.

Chordwise Pitching Axis Location

For cyclorotors with a large chord/radius ratio, the chordwise location of the pitching axis can have a significant influence on the performance [10]. This is because of the fact that the pitching axis location has a significant impact on the velocity and angle of attack at different chordwise locations on the blade, causing significantly different virtual camber/incidence effects. All the previous tests except the blade planform tests were performed with the pitching axis at the quarter-chord. A series of tests were conducted for pitching axis locations of 25, 35, and 45% chord for a 3-in.-radius rotor with 6.25 in. blade span and 2 in. blade chord, operating at a pitching amplitude of 40 deg (symmetric pitching).

To find the optimum location of the pitching axis, the variation of power loading with disk loading was plotted (Fig. 39). As shown in the figure, the power loading increased as the pitching axis location was moved from 25 to 35% chordwise locations. However, as the pitching axis location was moved from 35 to 45% chord, the power loading dropped significantly. Another key observation from this study is that, for a constant rotational speed, the thrust steadily dropped as the pitching axis was moved from 25 to 45% locations. For a rotational speed of 1600 rpm, the thrust dropped from almost 2.5 N at 25% location to 1.6 N at 45% location. It is a drop of 36% in thrust for just a 20% variation in pitching axis location. Therefore, as far as the pitching axis location is concerned, the rotor design for maximum thrust and maximum power loading would be completely different.

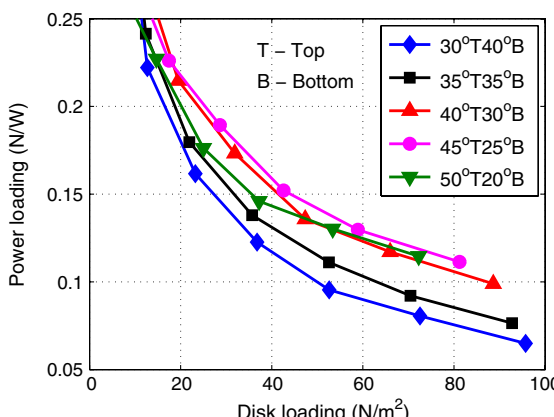


Fig. 38 Power loading versus disk loading for the 3-in.-radius rotor using 2-in.-chord 6.25-in.-span blades with asymmetric blade pitching.

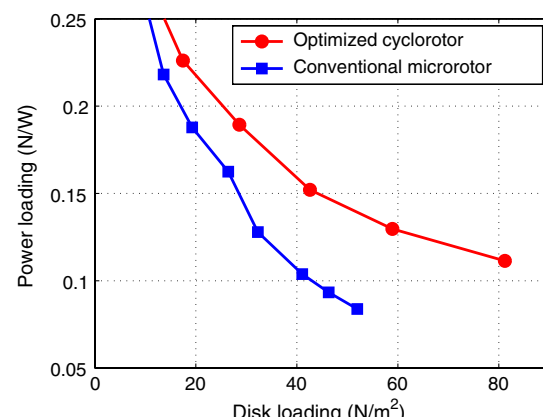


Fig. 40 Power loading for the optimized cyclorotor compared with a conventional microrotor.

Based on the rotor geometry and blade kinematics studies, the optimized cyclorotor (highest power loading for the same disk loading) had a 3 in. radius with a 6.25 in. blade span and 2 in. chord, operating at an asymmetric pitching of 45 deg at top and 25 deg at bottom, and the pitching axis at 25% chord. This optimized cyclorotor was compared with the performance of a conventional microrotor of a similar actuator area (diameter = 9 in., solidity = 0.137) [9] at the same disk loading (see Fig. 40). The power loading for the cyclorotor is significantly higher than the conventional rotor at all the disk loading values.

Conclusions

The present work has focused on optimizing the efficiency of a microscale cyclorotor through systematic performance measurements by varying the rotor geometry and blade kinematics. The rotor geometry parameters that were varied include the rotor radius, blade span, chord, and blade planform. These parameters, when systematically varied, identified substantial improvements in performance. Once the optimized cyclorotor geometry was obtained, further improvements in performance were achieved by varying the blade kinematic parameters, such as amplitude of blade pitch (symmetric and asymmetric pitching) and chordwise blade pitching axis location. The power loading of the optimized cyclorotor was higher than that of a conventional microscale rotor when compared at the same disk loading. The following are specific conclusions derived from this work:

1) Studies conducted by varying chord/radius ratio clearly showed that flow curvature effects (virtual camber/incidence) play a key role in the performance of the cyclorotor. The power loading of the cyclorotor is strongly dependent on the chord/radius ratio and not the radius itself (at a constant disk loading). The cyclorotor was shown to achieve higher values of power loading at higher chord/radius ratios. It was also significant to see that the optimum chord/radius ratio is a function of the pitching amplitude. The best chord/radius ratios for 40 and 25 deg pitching amplitudes were around 0.8 and 0.5, respectively.

2) The blade span studies showed that the blades with shorter spans perform better for the same disk loading, especially at lower pitching amplitudes (25 deg). However, for a 40 deg pitching amplitude, there was not much variation of power loading with blade span.

3) Rotor aspect ratio (span/diameter) studies clearly showed that it is important to operate at the optimum chord/radius ratio with a shorter blade span in order to maximize the power loading of the cyclorotor.

4) Cyclorotor performance improved with solidity up to about $\sigma \approx 0.4$. Also, if the solidity of the cyclorotor needs to be increased, the better approach is to increase the blade chord by keeping the number of blades fixed instead of increasing the number of blades using a smaller blade chord. This way, the rotor can take advantage of both the increase in total blade area and higher chord/radius ratio.

5) Blade planform studies showed that trapezoidal blades with moderate taper ratios can produce slightly higher power loading than rectangular blades at higher disk loadings. However, a large taper ratio degraded the performance.

6) Based on the blade kinematics studies, operating at higher pitching amplitudes improved power loading with optimum performance at 40 deg. Asymmetric pitching, where the pitch angle at the top is larger than the angle at the bottom, provided a better power loading than symmetric pitching. For a total peak-to-peak pitching angle of 70 deg, a 45 deg pitch angle at the top and 25 deg at the bottom produced the highest power loading. Shifting the pitching axis location away from the leading edge improved the performance, with the optimum pitching axis location being 25–35% chord. Since the rotors in the present study have a large chord-to-radius ratio, the location of the pitching axis and the asymmetry in pitch angle variation can significantly affect the aerodynamic performance of the cyclorotor because of the flow curvature effects.

7) The optimized cyclorotor had a significantly higher power loading compared to a conventional rotor when operated at the same disk loading. The optimum configuration based on all the tests was a four-bladed 3-in.-radius 6.25-in.-span rotor using a 2-in.-chord

NACA 0015 blade section with an asymmetric pitching of 45 deg at top and 25 deg at bottom, with the pitching axis at 25% chord.

Acknowledgments

This research was supported by the U.S. Army's Micro Autonomous Systems and Technology Collaborative Technology Alliance Center for Microsystem Mechanics with Joseph Mait [U.S. Army Research Laboratory (ARL)] and Chris Kroninger (ARL-Vehicle Technology Directorate) as the Technical Monitors. The authors would like to thank Raghav Gupta for his help in building the blades for the different cyclorotors tested. A revised version of this paper was presented at the American Helicopter Society Specialists' Meeting on Unmanned Rotorcraft and Network Centric Operations in 2011.

References

- [1] Ifju, P. G., Jenkins, D. A., Ettinger, S., Lian, Y., Shyy, W., and Waszak, M. R., "Flexible-Wing-Based Micro Air Vehicles," *AIAA 40th Aerospace Sciences Meeting and Exhibit*, AIAA Paper 2002-705, 2002.
- [2] Peterson, B., Erath, B., Henry, K., Lyon, M., Walker, B., Powell, N., Fowlkes, K., and Bowman, W. J., "Development of a Micro Air Vehicle for Maximum Endurance and Minimum Size," *AIAA 41st Aerospace Sciences Meeting and Exhibit*, AIAA Paper 2003-416, 2003.
- [3] Brion, V., Aki, M., and Shkarayev, S., "Numerical Simulation of Low Reynolds Number Flows Around Micro Air Vehicles and Comparison Against Wind Tunnel Data," *AIAA 24th Applied Aerodynamics Conference*, AIAA Paper 2006-3864, 2006.
- [4] Grasmeyer, J. M., and Keenon, M. T., "Development of the Black Widow Micro Air Vehicle," *AIAA 39th Aerospace Sciences Meeting and Exhibit*, AIAA Paper 2001-0127, 2001.
- [5] Keenon, M. T., and Grasmeyer, J. M., "Development of the Black Widow and Microbat MAVs and a Vision of the Future of MAV Design," *AIAA/ICAS International Air and Space Symposium and Exposition, The Next 100 Years*, AIAA Paper 2003-2901, 2003.
- [6] Pines, D., and Bohorquez, F., "Challenges Facing Future Micro-Air-Vehicle Development," *Journal of Aircraft*, Vol. 43, No. 2, 2006, pp. 290–305.
doi:10.2514/1.4922
- [7] Hein, B., and Chopra, I., "Hover Performance of a Micro Air Vehicle: Rotors at Low Reynolds Number," *Journal of the American Helicopter Society*, Vol. 52, No. 3, 2007, pp. 254–262.
doi:10.4050/JAHS.52.254
- [8] Chopra, I., "Hovering Micro Air Vehicles: Challenges and Opportunities," *Proceedings of American Helicopter Society Specialists' Conference, International Forum on Rotorcraft Multidisciplinary Technology*, Seoul, 2007.
- [9] Hrishikeshavan, V., and Chopra, I., "Design and Testing of a Shrouded Rotor MAV with Anti-Torque Vanes," *Proceedings of the 64th Annual National Forum of the American Helicopter Society*, Curran Associates, Inc., 2008, pp. 1456–1469.
- [10] Benedict, M., Jarugumilli, T., and Chopra, I., "Experimental Performance Optimization of a MAV-Scale Cycloidal Rotor," *Proceedings of the AHS Specialists' Meeting on Aeromechanics*, Curran Associates, Inc., 2010, pp. 119–135.
- [11] Benedict, M., "Fundamental Understanding of the Cycloidal-Rotor Concept for Micro Air Vehicle Applications," Ph.D. Thesis, Dept. of Aerospace Engineering, Univ. of Maryland, College Park, MD, Dec. 2010.
- [12] Yun, C. Y., Park, I. K., Lee, H. Y., Jung, J. S., Hwang, I. S., and Kim, S. J., "Design of a New Unmanned Aerial Vehicle Cyclocopter," *Journal of the American Helicopter Society*, Vol. 52, No. 1, 2007, pp. 24–35.
doi:10.4050/JAHS.52.24
- [13] Hwang, I. S., Hwang, C. P., Min, S. Y., Jeong, I. O., Lee, C. H., Lee, Y. H., and Kim, S. J., "Design and Testing of VTOL UAV Cyclocopter with 4 Rotors," *American Helicopter Society 62nd Annual Forum Proceedings*, Curran Associates, Inc., 2006, pp. 2100–2106.
- [14] Hwang, I. S., Hwang, C. S., and Kim, S. J., "Structural Design of Cyclocopter Blade System," *46th AIAA/ASME/ASCE/AHS/ASC Structures, Structural Dynamics and Materials Conference*, AIAA Paper 2005-2020, 2005.
- [15] Wheatley, J. B., and Windler, R., "Wind-Tunnel Tests of a Cyclogiro Rotor," NACA TN-528, May 1935.
- [16] Kirsten, F. K., "Cycloidal Propulsion Applied to Aircraft," *Transactions of the American Society of Mechanical Engineers*, Vol. 50, No. 12, 1928, pp. 25–47.

- [17] Boschma, J. H., "Modern Aviation Applications for Cycloidal Propulsion," *AIAA Aircraft, Technology Integration, and Operations Forum*, AIAA Paper 2001-5267, 2001.
- [18] Gibbens, R., "Improvements in Airship Control using Vertical Axis Propellers," *3rd AIAA Annual Aviation Technology, Integration, and Operations (ATIO) Forum*, AIAA Paper 2003-6853, 2003.
- [19] Gibbens, R., Boschma, J., and Sullivan, C., "Construction and Testing of a New Aircraft Cycloidal Propeller," *AIAA 13th Lighter-Than-Air Systems Technology Conference*, AIAA Paper 1999-3906, 1999.
- [20] McNabb, M., "Development of a Cycloidal Propulsion Computer Model and Comparison with Experiment," M.S. Thesis, Dept. of Aerospace Engineering, Mississippi State Univ., MS, Dec. 2001.
- [21] Nagler, B., "Improvements in Flying Machines Employing Rotating Wing Systems," U.K. Patent No. 280,849, issued Nov. 1926.
- [22] Iosilevskii, G., and Levy, Y., "Experimental and Numerical Study of Cyclogiro Aerodynamics," *AIAA Journal*, Vol. 44, No. 12, 2006, pp 2866–2870.
doi:10.2514/1.8227
- [23] Higashi, Y., Tanaka, K., Emaru, T., and Wang, H. O., "Development of a Cyclogyro-based Flying Robot with Variable Attack Angle Mechanisms," *IEEE/RSJ International Conference Proceedings on Intelligent Robots and Systems*, Curran Associates, Inc., 2006.
- [24] Yu, H., Bin, L. K., and Rong, H. W., "The Research on the Performance of Cyclogyro," *AIAA 6th Aviation Technology, Integration and Operations Conference*, AIAA Paper 2006-7704, 2006.
- [25] Benedict, M., Ramasamy, M., Chopra, I., and Leishman, J. G., "Performance of a Cycloidal Rotor Concept for Micro Air Vehicle Applications," *Journal of the American Helicopter Society*, Vol. 55, No. 2, 2010, p. 022002.
doi:10.4050/JAHS.55.022002
- [26] Benedict, M., Ramasamy, M., and Chopra, I., "Improving the Aerodynamic Performance of Micro-Air-Vehicle-Scale Cycloidal Rotor: An Experimental Approach," *Journal of Aircraft*, Vol. 47, No. 4, 2010, pp. 1117–1125.
doi:10.2514/1.45791
- [27] Sirohi, J., Parsons, E., and Chopra, I., "Hover Performance of a Cycloidal Rotor for a Micro Air Vehicle," *Journal of the American Helicopter Society*, Vol. 52, No. 3, 2007, pp. 263–279.
doi:10.4050/JAHS.52.263
- [28] Benedict, M., Sirohi, J., and Chopra, I., "Design and Testing of a Cycloidal Rotor MAV," *AHS International Specialists' Meeting Proceedings on Unmanned Rotorcraft: Design, Control and Testing*, 2007.
- [29] Benedict, M., Gupta, R., and Chopra, I., "Design, Development and Flight Testing of a Twin-Rotor Cyclocopter Micro Air Vehicle," *Proceedings of the 67th Annual National Forum of the American Helicopter Society*, Curran Associates, Inc., Virginia Beach, VA, 3–5 May 2009, pp. 135–148.
- [30] Migliore, P. G., Wolfe, W. P., and Fanuccif, J. B., "Flow Curvature Effects on Darrieus Turbine Blade Aerodynamics," *Journal of Energy*, Vol. 4, No. 2, 1980, pp. 49–55.
doi:10.2514/3.62459
- [31] Mandal, A. C., and Burton, J. D., "The Effects of Dynamic Stall and Flow Curvature on the Aerodynamics of Darrieus Turbines Applying the Cascade Model," *Wind Engineering*, Vol. 18, No. 6, 1994, pp. 267–282.
- [32] Lindenburg, C., "BLADMODE Program for Rotor Blade Mode Analysis," ECN Rept. ECN-C-02-050, Petten, The Netherlands, 2003
- [33] Hirsch, C. H., and Mandal, A. C., "Flow Curvature Effect on Vertical Axis Darrieus Wind Turbine Having High Chord-Radius Ratio," *Proceedings of the First European Wind Energy Conference*, H. S. Stephens and Associates, 1984, pp. 405–410.
- [34] Yang, K., Lakshminarayanan, V. K., and Baeder, J. D., "Simulation of a Cycloidal Rotor System Using an Overset RANS Solver," *Proceedings of the American Helicopter Society 66th Annual Forum*, Curran Associates, Inc., 2010, pp. 2341–2360.